Study of strongly correlated electrons in nanoscopic and bulk forms: some recent results

G Alvarez[1], K A Al-Hassanieh[2,3,4], F Popescu[5], C Şen[4], A Moreo[2,3] and E Dagotto[2,3]

[1] Computer Science and Mathematics Division and Center for Nanophase Materials Sciences, Oak Ridge National Laboratory, Oak Ridge, TN 37831, USA
[2] Condensed Matter Sciences Division, Oak Ridge National Laboratory, Oak Ridge, TN 37831, USA
[3] Department of Physics and Astronomy, University of Tennessee, Knoxville, TN 37996, USA
[4] National High Magnetic Field Laboratory and Department of Physics, Florida State University, Tallahassee, FL 32306, USA
[5] Department of Physics, Florida State University, Tallahassee, FL 32306, USA

Abstract

Recent progress in the numerical study of various strongly correlated electronic systems is reviewed. The study of transport in single molecule conductors and quantum dots is addressed with a recently proposed adaptive time-dependent density-matrix-renormalization group (DMRG). Experiments involving non-local spin control and their numerical simulation are also discussed. A section is devoted to recent efforts in the study of spin-fermion models for colossal magnetoresistive manganites, where we present insights on the effect of disorder and electron–phonon coupling. Finally, using a dynamical mean field approach, we review calculations in the area of diluted magnetic semiconductors that provides guidelines on how the Curie temperature could be increased in these itinerant ferromagnetic systems.

(Some figures in this article are in colour only in the electronic version)

1. Introduction

In several materials of technological interest the interactions between the electrons are collective, and these systems, referred to as strongly correlated electronic systems, display a broad range of interesting and important phenomena.

One example is the study of *electron transport through single-molecule conductors and quantum dots*. These nanostructures are not only candidates for novel potential applications, such as molecular electronics and quantum computing, but also provide well-controlled and tunable systems for studying interesting many-body effects. In this paper, we review recent results in this area, including the Coulomb blockade and Kondo effects in section 2.

Another example is the *colossal magnetoresistive (CMR) effect in manganites*. In recent years, much progress has been made in this context after the realization that several competing states, with quite different properties, are very close in energy in these compounds. As a consequence, small variations in carrier density, temperature, pressure, magnetic fields, and other variables often lead to giant responses. Moreover, the effect of quenched disorder appears to be important in understanding the colossal magnetoresistive effect, according to recent investigations that we review in section 3. This combination of strong correlation and disorder effects, and the simultaneous relevance of several degrees of freedom such as spin, charge, orbital, and lattice, lead to a plethora of unusual properties, with tremendous potential for applications.

In addition, we have included in this paper recent studies on *diluted magnetic semiconductors (DMSs)*, which are semiconductors where a small fraction of its atoms are magnetic. These materials are very promising for future applications in the area of spintronics. There are many formal similarities in the theoretical treatment of diluted magnetic semiconductors and the transition metal oxides mentioned above, justifying the inclusion of the former in this paper. Both classes of material present complex ground states, and this complexity leads to possible functionalities. Moreover, both systems require a careful treatment of electron interactions at the computational and theoretical level.

We will review recent results on these various correlated electron systems as studied with state-of-the-art computational techniques. For quantum dots, fundamental Hubbard models are considered. However, for CMR manganites and DMS materials more appropriate spin-fermion models have been developed that, even though they could still be considered only as phenomenological models, include all the relevant interactions at a microscopic level. These models have been accurately studied using Monte Carlo algorithms combined with exact diagonalization of the fermionic sector. We will also discuss future directions of research in each of these areas.

2. Recent studies of quantum dots and molecular conductors with computational techniques

2.1. Introduction

The rapidly developing investigations in the area of nanometre-scale systems and their con-comitant potential technological applications in real devices have induced considerable interest in the study of electron transport through single molecule conductors (MCs) and quantum dots (QDs). Due to the small size of these systems, Coulomb correlations are important. In addition, particularly in the case of single MCs, the electron–phonon coupling is also important, since molecules can change their shape and position relative to the leads as electrons enter or leave the system. This also has interesting effects on transport and other properties.

An important manifestation of electron correlations in nanostructures is the Coulomb blockade effect. The addition of an electron to a nanodevice is penalized by the Coulomb repulsion. Thus, the conductance is suppressed except for charge degeneracy points, where states with N and $N + 1$ electrons are degenerate, allowing for charge fluctuations. As a result, the conductance versus gate voltage curves present periodically spaced conductance peaks separated by low conductance valleys. This effect has been studied theoretically [1] and observed experimentally in both QDs [2] and single MCs [3, 4].

Another very interesting many-body effect is the Kondo effect. When an odd number of electrons occupy the device, conduction electrons in the leads screen their combined local magnetic moment. An overall singlet is formed. The antiferromagnetic correlations between the localized and conduction electrons lead to the formation of a resonance in the local

density of states of the device. This resonance, the Kondo resonance, provides a channel for electron transport. The energy scale of this effect is defined as the Kondo temperature T_K. Electron transport through the Kondo resonance was predicted theoretically [5–7], and has been observed experimentally in lithographic quantum dots [8], single molecules [3, 4, 9], carbon nanotubes [10], and other nanostructures.

More elaborate systems that show competitions between different correlation effects or more exotic Kondo effects have been studied. In the case of coupled QDs, the Kondo correlations between each dot and its neighbouring lead compete with the antiferromagnetic correlations between the two dots [11–13]. Ferromagnetic correlations have been predicted for coupled double-level QDs in the quarter-filling regime [14]. Integer-spin Kondo effect has been observed in multilevel QDs where the T_K is enhanced at the singlet–triplet degeneracy points [15]. Orbital Kondo effect, in addition to spin Kondo effect, has been observed in carbon nanotube based QDs. The conduction electrons in the leads screen both the orbital and spin degrees of freedom of the QD. When orbital and spin degeneracies are present simultaneously, a strongly enhanced Kondo effect obeying the $SU(4)$ symmetry is observed [16]. In addition to electronic correlation effects, vibrational effects in single MCs have received much theoretical attention [17–19] and have been observed in different experiments [20, 21].

2.2. DMRG method to study conductances

For a conceptual understanding of these complex systems, it is imperative to develop models and unbiased many-body methods that rely on a minimal number of assumptions in order to accurately handle both strong Coulombic and electron–phonon couplings. Several numerical techniques are being used to study electron transport in nanostructures (see [22] and references therein). The minimal model to describe QDs and single MCs is the one-level Anderson impurity model. This model can be written as $H = H_D + H_{leads} + H_{D-leads}$, where H_D, the Hamiltonian of the QD (or molecule), is given by $H_D = V_g n_d + U n_{d\uparrow} n_{d\downarrow}$. The first term represents the location of the energy level of the QD controlled by the gate voltage V_g. The second term represents the Hubbard repulsion between electrons of opposite spins occupying the QD. $n_d = n_{d\uparrow} + n_{d\downarrow}$ is the number of electrons at the dot. H_{leads} is the Hamiltonian of the leads, modelled, in the results shown below, as ideal tight-binding chains. $H_{D-leads}$ connects the dot to the leads. It can be written as $H_{D-leads} = -t' \sum_\sigma [c_{l\sigma}^\dagger d_\sigma + c_{r\sigma}^\dagger d_\sigma + \text{h.c.}]$, where t' is the amplitude for the electronic hopping between the QD and the leads. $d_\sigma^\dagger$ creates an electron with spin σ at the dot while $c_{l\sigma}^\dagger$ ($c_{r\sigma}^\dagger$) creates an electron with spin σ at the last (first) site of the left (right) lead, if sites are numbered form left to right.

As an example of a powerful numerical technique used to study this type of system, we focus briefly on a recently proposed adaptive time-dependent DMRG-based technique to study nanotransport [22] (see also [23]). This technique has the advantages of being accurate, flexible enough to treat a wide spectrum of problems, and independent of any linear response assumptions. Thus, is can be used to study both equilibrium and non-equilibrium problems.

Figure 1 outlines the basic steps of the technique. In figure 1(a), a schematic representation of the geometry used is shown. The system in general consists of a relatively small interacting region connected to two leads. The leads are modelled by tight-binding Hamiltonians. The ground state at time zero is calculated at zero bias. Then, a finite bias ΔV is applied between the two leads and the wavefunction is evolved in time. The resulting current J is measured as a function of time. The current typically shows a fast increase from zero followed by a steady-state plateau. The value of the current at the steady state is used to calculate the conductance. Figures 1(b) and (c) show the exact results for $J(t)/\Delta V$ (in units of e^2/h) versus time (in units of $\hbar/t_{leads}$ where t_{leads} is the hopping parameter in the leads) for the case of non-
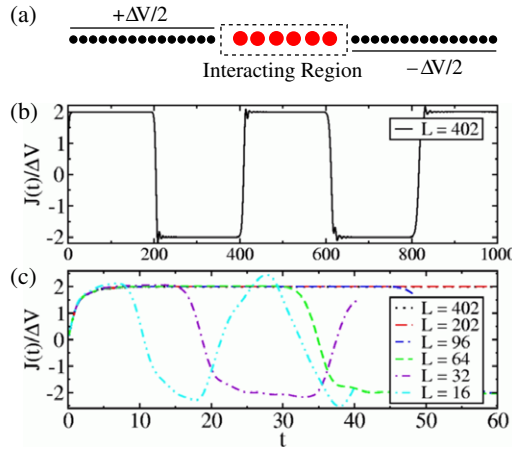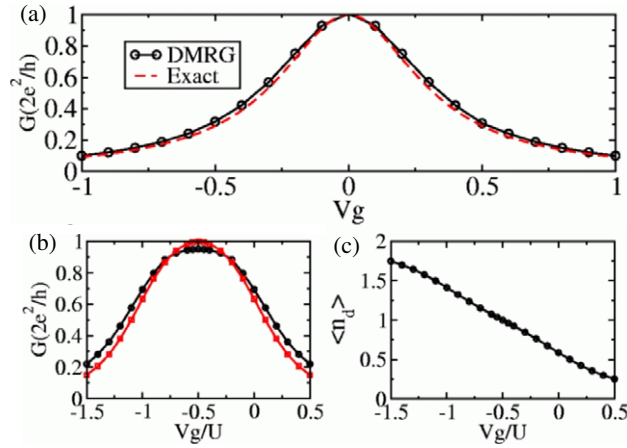
Figure 1. Adaptive time-dependent DMRG technique to study nanotransport. (a) Schematic representation of the geometry used. The leads are modelled by tight-binding Hamiltonians. The ground state at time zero is calculated at zero bias. Then, a finite bias ΔV is applied between the two leads and the resulting current is measured. (b) Exact results for $J(t)/\Delta V$ (in units of e^2/h) versus time (in units of $\hbar/t_{\text{leads}}$) for a cluster of length $L = 402$. $J(t)/\Delta V$ shows clear steady-state plateaus at $\pm 2e^2/h$. The periodic changes in the current direction are caused by its reflection at the open boundaries of the cluster. (b) $J(t)/\Delta V$ obtained with decreasing L. The steady-state plateau is obtained even with $L = 32$. The current is quasiperiodic with a period proportional to L (from [22]).

interacting electrons and one quantum dot, obtained with clusters of different lengths (L) and $\Delta V = 0.001$. Figure 1(b) shows $J(t)/\Delta V$ obtained with a large cluster ($L = 401$). $J(t)/\Delta V$ presents clear steady-state plateaus at $\pm 2e^2/h$. The large-scale periodic changes in the current direction are caused by its reflection at the open boundaries of the cluster. Figure 1(c) shows $J(t)/\Delta V$ obtained with decreasing L. The steady-state plateau is obtained even with $L = 32$. The current is quasiperiodic with a period proportional to L.

Figure 2 shows the conductance G versus V_g for the 1QD case obtained using the procedure described above. Figure 2(a) shows G deduced from the behavior of the current obtained with the DMRG method for a single 'non-interacting' QD, namely, one having $U = 0$. It is expected that the maximum value of G will be obtained when the level in the dot is aligned with the Fermi level of the leads, and this occurs in our case at $V_g = 0$. The DMRG results confirm this expectation. As V_g changes away from 0, G is expected to decrease symmetrically, and this is indeed shown in figure 2(a). In fact, the results at non-zero gate voltage are also in excellent quantitative agreement with the exact results. Figure 2(b) shows the results obtained for an intermediate value of U, namely $U = 1$. These results are compared with the conductance obtained using the Friedel sum rule (FSR), $G = \frac{2e^2}{h} \sin^2(\frac{\pi}{2} \langle n_d \rangle)$. The shape of the curve is the expected one for the regime considered here: the intermediate value of U does not locate our investigations deep in the Kondo regime, with sharply defined integer charge at the dot, but more into the so-called mixed-valence region. This can be deduced from the value of the dot charge versus V_g, shown in figure 2(c). With increasing U and/or decreasing t', sharper charge steps are formed, but the Kondo cloud size increases, thus requiring larger clusters to be used.

2.3. Non-local spin control

As an example of more elaborate nanosystems, we discuss briefly the results of recent important experiments involving non-local spin control [25]. We also discuss our numerical results

Figure 2. Adaptive time-dependent DMRG results in the case of one QD. (a) DMRG and exact results for G versus V_g in the case of one non-interacting QD. The DMRG results are obtained with $L = 64$ and number of states $M = 300$. G is obtained from the value of the steady-state current plateau. The exact results are for infinite leads. The plots show a resonant tunnelling peak with a full width at half maximum (FWHM) equal to $4t'^2$ at $V_g = 0$. (b) G for one interacting QD. Circles show G obtained by averaging the current over an interval of time corresponding to the steady state. Squares show G obtained from $\langle n_d \rangle$ using the Friedel sum rule (FSR). G has the shape of the expected Kondo or mixed-valence plateau centred at $V_g = -U/2$. This feature would become sharper by increasing U and/or decreasing t'. The results shown here were obtained using $U = 1.0$, $t' = 0.4$, $L = 128$, and $M = 300$. (c) The dot occupation $\langle n_d \rangle$ for the same parameters (from [22]).
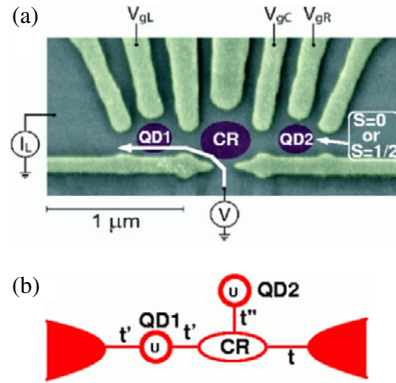
Figure 3. (a) Experimental setup used in the non-local spin control experiments. The system consists of two QDs (labelled QD1 and QD2) coupled through an open conducting central region (CR). The arrow indicates the direction in which bias is applied and conductance is measured. (b) Illustration of the model used in our numerical study. An Anderson impurity model is used to describe QD1 and QD2. QD2 is coupled to CR through the hopping parameter t''. Note that QD2 is side coupled to the direction in which the conductance is measured, thus a Fano antiresonance is quite natural in this system (from [24]).

simulating those experiments [24]. The experimental setup is shown in figure 3(a). The system consists of two similar QDs (labelled QD1 and QD2) coupled through an open conducting central region (CR). A finite bias is applied to QD1 as well as to the CR, while QD2 is kept at a constant gate potential. The differential conductance of QD1 is then measured for different

charge states of QD2 and different values of its coupling to the CR. The main result was the suppression and splitting of the Kondo peak in QD1 by changing the occupancy of QD2 from an even to an odd number of electrons and by increasing its coupling to the CR. A Ruderman–Kittel–Kasuya–Yosida (RKKY) interaction between the QDs was suggested as an explanation for the observed effects. Figure 3(b) shows the model used to simulate the experiment. The Anderson impurity Hamiltonian is used for both QDs. The calculations were carried out using the exact diagonalization plus Dyson equation technique [26]. Our numerical results nicely reproduced the experimental results. The system was also analysed using a simple circuit model, where the system is treated as a circuit of a serial QD (QD1) and a side-coupled QD (QD2) connected in series. The results of this simple analysis also reproduced the experimental results. The main conclusion of the numerical study was the following. The effects observed experimentally can also be explained as a result of the destructive interference of the two paths that an electron can take: a direct path through CR and QD1, and an indirect path through CR, QD2, CR and QD1. This so-called Fano antiresonance is quite natural in systems with side-coupled QDs.

2.4. Molecular conductors

As mentioned above, in the case of single MCs, in addition to the Coulomb interactions, the electron–phonon coupling is also important and can have interesting effects on transport properties. Let us discuss briefly the conductance of a molecule with centre of mass motion [17]. This system was studied numerically using the exact diagonalization plus Dyson equation technique. The molecule is allowed to oscillate between the two leads. It is clear that the molecule–leads tunnel barriers depend on the molecule displacement from its equilibrium position. The molecule is modelled using the Anderson–Holstein model. The Hamiltonian that connects the molecule to the leads can be written as $H_{M-leads} = t'[1 - \alpha(a + a^{\dagger})] \sum_{\sigma} (d_{\sigma}^{\dagger} c_{l0\sigma} +$ h.c.) $+ t'[1 + \alpha(a + a^{\dagger})] \sum_{\sigma} (d_{\sigma}^{\dagger} c_{r0\sigma} + $ h.c.). In this model, $d_{\sigma}^{\dagger}$ creates an electron with spin σ in the molecule, t' is the hopping parameter between the molecule and the leads, and α is a parameter that carries the dependence of t' on the molecule displacement from its equilibrium position $\hat{x}$ (note the opposite signs in this dependence for the two leads, caused by the molecules' centre of mass oscillations). This displacement can be written in terms of the phononic operators as $\hat{x} = (a + a^{\dagger})$. The main result observed was the presence of a conductance dip at $V_g = -U/2$, for both the interacting and non-interacting electronic cases. In the following, we present an explanation of the conductance dip. The reasoning starts by noting that $H_{M-leads}$ can be rewritten as a sum of two channels contributing to the overall molecule–leads connection. The first term, $t'\alpha(a + a^{\dagger}) \sum_{\sigma} (d_{\sigma}^{\dagger} c_{r0\sigma} - d_{\sigma}^{\dagger} c_{l0\sigma} + $h.c.), represents a phonon-assisted tunnelling channel, i.e. the electron absorbs (emits) a phonon upon entering the molecule and, then, emits (absorbs) a phonon upon leaving. The two channels were studied separately by keeping only the relevant term in $\hat{H}_{M-leads}$. The conductance and the phase carried by each channel were calculated. It was found that, for $V_g = -U/2$, the conductance of each of the channels is $2e^2/h$ and the phase difference is π, leading to a perfect cancellation in the overall conductance. This interference effect is independent of the electron–electron interaction and, thus, the cancellation should still be present for $U = 0$, as obtained numerically.

These systems provide a unique well-controlled and tunable playground, both for testing many-body theories and exploring new and exotic many-body effects. Some of these effects are very difficult or even impossible to realize in bulk system. In parallel with the huge experimental advances, reliable many-body, particularly numerical, techniques are essential to understand these increasingly interesting systems. This is an area of research with a bright future and surely with many interesting surprises waiting to be discovered.

3. Theoretical progress in colossal magnetoresistance

3.1. Introduction

An important open problem in the area of transition metal oxides is the explanation of the colossal magnetoresistance (CMR) effect that appears in the Mn oxides that are widely referred to as manganites. These compounds present a rich phase diagram with a variety of competing states which are stabilized by changing the carrier concentration using a standard chemical doping process involving ions with different valences, or by varying the carrier bandwidth via isovalent doping. Among the low-temperature ground states in manganites there appears a ferromagnetic (FM) metallic phase and several antiferromagnetic/charge/orbital ordered insulating states. For the compounds with intermediate or small Curie temperatures, the experimentally obtained resistivity versus temperature curves present a sharp peak, which occurs precisely at the transition toward ferromagnetism. In the vicinity of this peak, the CMR effect is observed, which consists of enormous changes in the resistivity upon the introduction of relatively small magnetic fields. Technological applications of CMR compounds in the magnetic recording industry will still need a substantial increase of the currently available critical temperatures where the large magneto effects occur. However, the physics behind this remarkable CMR phenomenon defines a challenging basic-science problem that has attracted the attention of the condensed matter community.

The explanation of the CMR effect is one of the most important goals of theoretical investigations in the manganite context. It has been shown that the standard double exchange (DE) model was not sufficient to understand these materials [27]. In fact, a DE model cannot even produce an insulator at high temperatures, in the realistic regimes of electronic densities [28], and this pointed toward the importance of other couplings, such as electron–phonon, for a proper description of these compounds. Progress was later made with the realization that manganite models have tendencies toward mixed phase regimes, typically involving metallic and insulating states in coexistence [29, 30]. This discovery was possible only after the DE model and its close variations were studied with unbiased computational methods beyond mean-field approximations. Inhomogeneous states with a variety of length scales appear frequently in these studies and powerful computational tools are clearly needed to fully understand CMR materials [31]. The theoretical discovery of phase separation tendencies [32] was followed by an enormous experimental effort that confirmed the relevance of mixed states in most of the CMR compounds (for a review see [33]). Percolative pictures were envisioned to understand these materials. Model calculations by Mayr *et al* [34] and Burgy *et al* [35, 36], using simplified spin systems and random resistor networks, revealed a phenomenology very similar to that of real CMR materials in the regime of couplings and electronic densities where metallic and insulating states were in competition.

This initial effort using simple models was followed by calculations of resistivities in the more realistic, although still simplified, one-orbital model for manganites. Verges *et al* [37] numerically showed that an insulator can appear at intermediate and large temperatures if the electron–phonon coupling λ is large enough. In this model, the two tendencies in competition at low temperatures are *both* ferromagnetic, and they only differ in the character of the charge distribution (uniform versus localized). The results considering only FM phases (metallic and insulating) cannot solve the entire CMR issue, since often the competition in experiments is between a ferromagnet against an antiferromagnetic/charge/orbital ordered state. However, those results are sufficiently interesting and challenging that they will be reviewed in detail here following closely [38]. Moreover, they could be of relevance to important Mn oxides such as $La_{0.7}Ca_{0.3}MnO_3$, which at least naively seem well separated from charge ordered states in

the phase diagrams. Recently, Kumar and Majumdar [39, 40] observed that the clean limit results of [37] are much enhanced by including on-site quenched disorder, together with a robust electron–phonon coupling.

Here we will review recent important progress related to the CMR problem. We will show that by increasing the electron–phonon coupling three regions are observed. First, for small electron–phonon coupling the system is metallic. As the electron–phonon coupling is increased past a critical value, a region in parameter space is found where the system has a metal insulator transition at finite temperature. If the electron–phonon coupling is too large the system becomes insulating for all temperatures. Even though the previous scenario is correct, the Hamiltonian parameters have to be tuned carefully to obtain a 'critical' region with a metal insulator transition at finite temperature. We show that the critical region is much enhanced when quenched disorder is added.

3.2. Model and methods

The Hamiltonian for the one-orbital model is

$$
\begin{aligned}
H_{1b} = -t \sum_{\langle ij \rangle, \alpha} (c_{i,\alpha}^\dagger c_{j,\alpha} + \text{h.c.}) - J_\text{H} \sum_{i,\alpha,\beta} c_{i,\alpha}^\dagger \vec{\sigma}_{\alpha,\beta} c_{i,\beta} \cdot \vec{S}_i \\
- \lambda t \sum_{i,\gamma,\alpha} (u_{i,-\gamma} - u_{i,\gamma}) c_{i,\alpha}^\dagger c_{i,\alpha} + t \sum_{i,\gamma} (u_{i,\gamma})^2 \\
+ \sum_{i,\alpha} (\Delta_i - \mu) n_{i,\alpha},
\end{aligned}
\tag{1}
$$

where $c_{i,\alpha}^\dagger$ creates an electron at site i with spin α, $\sigma_{\alpha,\beta}$ are the Pauli spin matrices, $\langle ij \rangle$ indicates summing over nearest-neighbour sites, and t is the nearest-neighbour hopping amplitude for the movement of electrons (t also sets the energy unit, i.e. $t = 1$ in all of the results below). The first and second terms are the standard for a double exchange model, with $\vec{S}_i$ being a classical localized spin that represents the t_{2g} degrees of freedom. The third term in the Hamiltonian accounts for the energy corresponding to the lattice–carrier interaction, with λ being the strength of the electron–phonon coupling. $u_{i,\gamma}$ are the distortions (lattice displacements) of the oxygen atoms surrounding a Mn ion at site i. The index γ in three dimensions (two dimensions) runs over three (two) directions x, y and z (x and y). The tendency toward increasing the magnitude of the lattice distortions is balanced by the fourth term in the Hamiltonian, which represents the stiffness of the Mn–O bonds. Since the study of quantum phonons in this context is not possible with currently available algorithms, the oxygen displacements are considered classical, an approximation widely used in studies of manganites [33]. Finally, the last term corresponds to the quenched disorder, which here it is introduced in the form of random site energies. Δ_i represents the strength of the disorder at a given site, and these numbers are chosen from a bimodal distribution of width 2Δ with mean 0. The overall electronic density n is controlled with the help of a chemical potential μ added to the last term in the Hamiltonian.

For manganites, J_H is known to be large, and to simplify our study we consider the limit of $J_H \to \infty$, which has been shown to preserve the essential physics of manganites [33]. In this limit, the spin of the e_g-electron perfectly aligns along the localized t_{2g}-spin direction. For an infinite Hund coupling, the system is particle–hole symmetric with respect to density $n = 0.5$. Thus, results at densities n and $1 - n$ are equivalent.

This Hamiltonian is solved using the standard exact diagonalization of the quadratic fermionic sector for a given spin background [33, 30]. The procedure, then, consists of integrating the t_{2g} spins (assumed to be classical) by means of a Monte Carlo algorithm. Details have been widely discussed in previous studies and they will not be repeated here [33, 30].
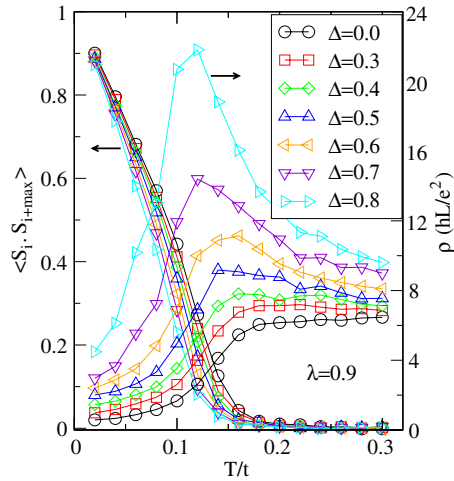
Figure 4. Monte Carlo results obtained using a $4 \times 4 \times 4$ lattice. Shown are the resistivity and spin–spin correlations, the latter at the maximum allowed distance $(2\sqrt{3})$, versus temperature, working at $\lambda = 0.9$, $n = 0.3$, and for the disorder strengths Δ indicated. The results shown are mainly for one configuration of quenched disorder, but as many as ten configurations were used in particular cases of temperatures and Δ, and no substantial deviations were observed between disorder configurations (from [38]).

The resistivity ρ has been calculated by taking the inverse of the mean conductivity σ, where the latter is related to the conductance G by $G = \sigma L^{d-2}$, with d being the dimension and L the linear size of the lattice. The calculation of the conductance G has been carried out following the approach extensively discussed before by Verges [41]. The use of the resistivity notation is to facilitate the interpretation of results and comparison with experiments, namely we do not claim to have observed ohmic behavior in our small system simulations. The units used for the resistivity are $[h/e^2]$ in two dimensions, and $[h/e^2] \times L$ in three dimensions. To restore the proper units to our results, the real lattice spacing of Mn oxides must be used.

3.3. Resistivity

The discussion of our computational results starts at the electronic density $n = 0.3$ (equivalent to $n = 0.7$, due to symmetry). Figure 4 is a typical example of the resistivity curves. Shown are both the spin–spin correlation at the maximum distance possible in the cluster under study and the resistivity, working at a fixed electron–phonon coupling $\lambda = 0.9$, and varying the strength of the quenched disorder Δ. In the clean limit, $\Delta = 0$, there is a rapid change in resistivity near the transition to ferromagnetism. This is a typical pure double-exchange behavior: in the absence of a sufficiently strong λ, quenched disorder, or other couplings that may lead to competing states, then a metal is obtained at temperatures above the Curie temperature. As already clearly established in this field, pure double-exchange models are not enough to address the physics of the CMR materials. However, note the dramatic effect of quenched disorder on the resistivity, as shown in figure 4. Disorder can induce a peak in the resistivity that much resembles experimental results for typical CMR materials. Even for the small systems studied here, the ratio of resistivities between its maximum and minimum values is as large as ∼6 for $\Delta = 0.7$. Note the correlation between the peak location and the temperature where ferromagnetic order appears (signalled in our calculations by the value of the spin–spin correlation at the largest possible distance in the cluster under investigation).
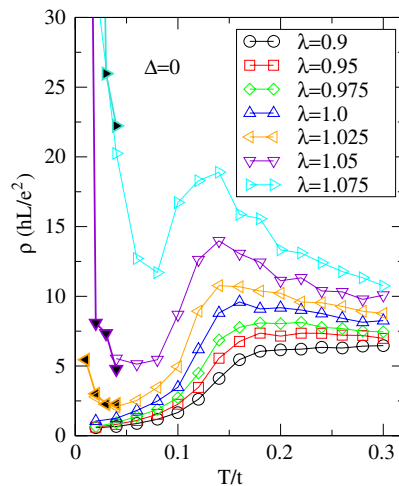
Figure 5. Influence of the electron–phonon coupling λ on the resistivity curves in the clean limit $\Delta = 0$, considering a $4 \times 4 \times 4$ lattice, and $n = 0.3$ (from [38]).

Although a variety of previous theoretical and experimental investigations have convincingly shown the importance of quenched disorder in the CMR context, nevertheless it is interesting to observe that a resistivity peak can also be found by varying λ even in the clean limit $\Delta = 0$, as shown in figure 5. There seems to exist a qualitative relation between increasing Δ at small λ and simply increasing λ at $\Delta = 0$. However, there is an important difference between the two cases: observing the resistivity peak in the clean limit requires a *fine tuning* of λ. For a non-zero Δ, the range of couplings with a resistivity peak is much wider (see below in the $n = 0.1$ subsection for a more detailed discussion). Fine tuning is not compatible with the CMR effect since the phenomenon appears in a large number of manganese oxides, with a distribution of λ. For a discussion on the increase in the resistivity at very low temperature in figure 5 see [38].

The resistivity curves with peaks at intermediate temperatures (figures 4 and 5) resemble the experimental data corresponding to real manganites. Even if only qualitatively, the similarity of the Monte Carlo data in figures 4 and 5 with experimental observations is excellent.

3.4. Magnetoresistance

The study would not be complete without the investigation of the effect of a magnetic field. We will show that when a magnetic field is included, samples that present a peak in the resistivity also present a large magnetoresistance effect. In this subsection, $n = 0.1$ will be considered (as already noted, $n = 0.9$ is the same, via symmetry considerations for the model used). Several of the effects discussed at the realistic density $n = 0.3$ in the previous section were found to be magnified by reducing the electronic density. Moreover, the lattice to be shown is now two dimensional, to illustrate the similarity systematically found between results in two and three dimensions.

The effect of magnetic fields at $n = 0.1$ is very pronounced (see figure 6), resembling the magnitude of the CMR effect in real materials. The region in the vicinity of the resistivity peak is the most affected. The magnetoresistance ratios are as large as those reported in the real Mn oxides with the largest CMR effects. The trade-off is that the effect occurs only in a small
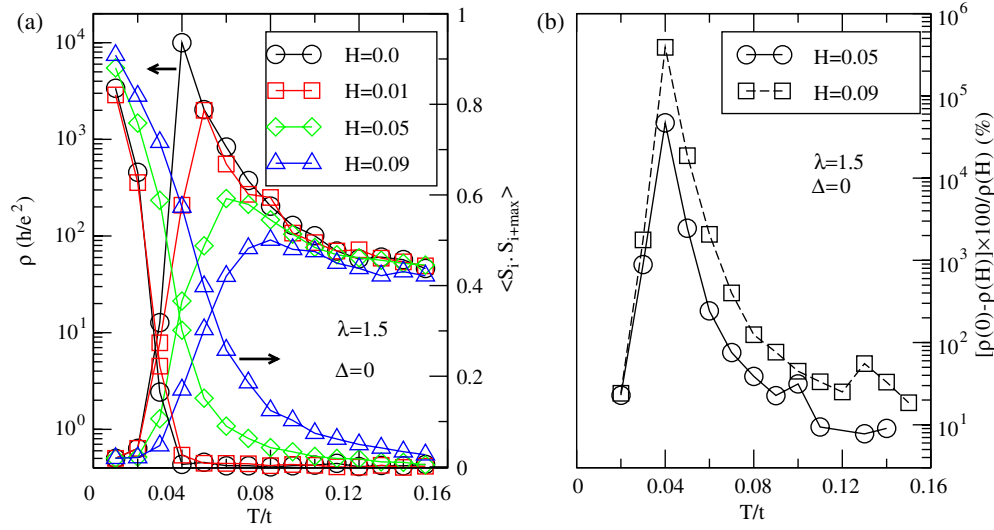
Figure 6. (a) Influence of magnetic fields on the resistivity curve and on the spin–spin correlation at the maximum allowed distance ($4\sqrt{2}$) on an 8×8 lattice, in the clean limit $\Delta = 0$. (b) Magnetoresistance ratios versus temperature, calculated for two representative magnetic fields. In both (a) and (b), $\lambda = 1.5$ and $n = 0.1$ (adapted from [38]).

window of λ, but this range, as well as the magnetoresistance value, can be further enlarged by adding quenched disorder.

The research effort discussed in previous publications by our group and others, and reviewed in this section, reached several goals. First, it confirmed the existence of a large peak in the resistivity versus temperature for the one-orbital model for manganites, including a robust electron–phonon coupling. This confirmation was obtained using unbiased techniques to estimate transport properties, and also with a Monte Carlo method that considers the complete Fermi sector without approximations. Second, a comprehensive analysis of the influence of couplings, quenched disorder strength, and electronic density was obtained. Although the last word has not still been said about the CMR phenomenon, considerable progress in its theoretical study has been reached in recent years. In particular, it is clear that the competition of two phases is crucial to have a colossal magnetoresistance.

4. Diluted magnetic semiconductors: a dynamical mean-field study of a two-band model

4.1. Introduction

Dynamical mean-field theory (DMFT) of strongly correlated electron systems replaces the full lattice of atoms and electrons with a single impurity atom imagined to exist in a bath of electrons [42, 43]. While the theory maps the lattice model onto an impurity model, hence simplifying the spatial dependence of correlations among electrons, it still accounts fully for the their temporal dynamics, that is, for the local quantum fluctuations which are missing in an usual mean-field treatment [44]. Besides its conceptual value of providing a quantum analogue of the classical mean-field approach, the DMFT mapping of the lattice model onto an impurity model has important implications in approaching several complicated strongly correlated electron systems. Among such systems, the diluted magnetic semiconductors (DMSs), which are materials in which a small fraction x ($\approx$1–10%) of non-magnetic elements is replaced

by magnetic impurities, attracted a substantial attention in the last decade due to their potential application in spintronic devices with new functionalities [45, 46]. Technologically, a semiconductor doped with magnetic atoms, usually Mn, which combines both semiconductor properties and magnetism, was shown experimentally to exhibit ferromagnetic transition temperatures that led to expectations that such materials could be extensively applied in spintronics. Due to significant improvements in molecular beam epitaxy (MBE) techniques, a ferromagnetic transition temperature (T_C) of about 170 K has been recently recorded experimentally in Mn-doped GaAs [47]. In addition to its potential technological applications, the ferromagnetism of $Ga_{1-x}Mn_xAs$ is a fundamental condensed matter problem as it represent a challenge to theory due to the combined presence of correlations and quenched disorder. The Mn dopants in GaAs serve the dual role of magnetic impurities that produce the local magnetic moments and of acceptors producing basically one hole per Mn atom. In turn, the density of charged carriers is itself a fraction ($\sim$10%) of the Mn concentration due to the strong localization at As antisite defects [48].

4.2. Study of two bands

Using dynamical mean-field theory (DMFT), in previous publications to be reviewed here we have studied the ferromagnetic transition temperature (T_c) of a two-band model for diluted magnetic semiconductors (DMSs), varying the coupling constants, hopping parameters, and carrier densities. The DMFT treatment discussed here follows closely the results of [49]. We found that T_C is optimized at all fillings p when both impurity bands (IBs) fully overlap in the same energy range, namely when the exchange couplings, as well as the bandwidths, are identical. The optimal T_C is found to be about twice as large as the maximum value obtained in the one-band model, showing the importance of multiband descriptions of DMSs at intermediate couplings. Within DMFT, pioneering calculations for two-band models based on double-exchange Hamiltonians already exist [50]. However, those calculations focused on special cases, while the present DMFT effort is more general, with two $s = 1/2$ bands and arbitrary couplings, hoppings, and carrier densities. One of our main results is that T_C can be substantially raised by considering multiband systems since at intermediate couplings the maximal T_C at carrier filling $p \cong x$ is approximately twice as large as the highest T_C obtained in the single-band model at filling $p \cong x/2$. The qualitative reason is that the IBs cooperate to raise T_C for values of the chemical potential μ where these bands partially or fully overlap [49].

It is known that in Mn-doped GaAs, the Mn ions substitute for Ga cations and contribute itinerant holes to the valence band. The Mn ions are in the Mn^{2+} state and have a half-filled d shell which acts as a $S = 5/2$ local moment. Since the valence band of GaAs is p-like, a strong spin–orbit (SO) coupling between the angular momentum $\mathbf{l} = 1$ of the p orbital and the hole spin degree of freedom $\mathbf{s} = 1/2$ produces low- and high-energy bands with angular momentum $\mathbf{j} = 1/2$ and $3/2$, respectively. A robust SO split between these bands ($\Delta_{SO} \approx 340$ meV) causes the holes to populate the $\mathbf{j} = 3/2$ state, which itself is split by the crystal field into an $m_j = \pm 3/2$ band with heavy holes and an $m_j = \pm 1/2$ band with light holes. Such a strong Δ_{SO} induces an anisotropic carrier-mediated interaction among the Mn ions that produces frustration in their ferromagnetic order [51], therefore reducing T_C. While theoretical models might consider realistic effective masses for holes ($m_h \approx 0.5m_e$ and $m_l \approx 0.07m_e$ with a ratio $r = m_l/m_h \approx 0.14$; m_e is the electron mass), studies have shown that T_C is maximized when giving similar masses to both heavy and light sectors [50]. The difference in band masses may induce magnetic frustration as the kinetic energy $\hat{K} = \sum_{\mathbf{k}} \hat{c}^\dagger_{\mathbf{k},\alpha} \epsilon_{\mathbf{k},\alpha\beta} \hat{c}_{\mathbf{k},\beta}$ is only diagonalized when the angular momentum is quantized along the momentum direction [52]. Otherwise, with an arbitrary quantization direction at $r = 1$ the magnetic frustration is absent. This argument

may serve as an explanation for the recorded high values of T_C up to 250 K [53], since in delta-doped GaAs the reduction of the magnetic frustration might be associated with the restriction of Mn ions in two-dimensional planes, such a restriction allowing for the orientation of the Mn moments perpendicular to the plane.

Within DMFT, the weak-coupling quadratic dependence of T_C with the exchange J is properly captured by using a one-band model for DMSs [54]. However, the predicted T_C versus J dependence at large J is almost a flat plateau, a result that has in turn been contradicted by the Monte Carlo (MC) simulations of finite clusters that correctly handle the random Mn distribution. While for J comparable with the hopping t both techniques reach similar conclusions, at large J the MC techniques show the decay of T_C due to carrier localization [55, 56].

With two active bands that basically define its ferromagnetism, the Mn-doped GaAs becomes a subject of particular interest since the consideration of several active bands in real DMS materials beyond mean-field approximations is essential in understanding the ferromagnetism of DMSs and the occurrence of T_C close to room temperature [57, 58]. To account for both active bands, we introduced a simple two-band model based on the Hamiltonian:

$$\mathcal{H} = -\sum_{ll',\langle ij\rangle\alpha} t_{ll'}(c_{l',j\alpha}^{\dagger} c_{l,i\alpha} + \text{H.c.}) - 2\sum_{l,I} J_{H,l}\mathbf{S}_I \cdot \mathbf{s}_{l,I}, \tag{2}$$

where l, l' (=1, 2) are the band indices (not to be confused with angular momentum), i, j label nearest-neighbour sites, $c_{l,i\alpha}$ creates a hole at site i in the band l, $\mathbf{s}_{l,i} = c_{l,i\alpha}^{\dagger}(\sigma_{\alpha\beta}/2)c_{l,i\beta}$ is the spin-operator of the mobile hole ($\hat{\sigma}$ = Pauli vector), α and β are spin indices, $J_{H,l}$ is the Hund coupling between the core spin and the electrons of band l, and $\mathbf{S}_I$ is the spin of the localized Mn ion at randomly selected sites I, assumed here classical ($\mathbf{S}_i = S\mathbf{m}_i$, where $\mathbf{m}_i$ is a randomly oriented unit vector). While for $l = l'$ we refer to t_{ll} as the direct-orbital hopping ($\equiv t_l$), for $l = l'$ the off-diagonal hopping $t_{ll'}$ is referred to as the interorbital hopping ($t_{ll'} = t_{l'l}^*$) [59]. The two active bands couple when the carriers from both bands simultaneously scatter the same core spin and when the bands exchange carriers via the off-diagonal hopping. While the first coupling clearly causes an increase in T_C when the bands overlap within the same energy interval, namely when $J_{H,l}$ are closed, the exchange effect is expecting to produce its further boost [59].

4.3. Results

The DMFT technique applied to the Hamiltonian, equation (2), allows us to obtain the interacting density of states (DOS) and an implicit equation for T_C. The T_C is then extracted from the structure of Matsubara frequencies numerically. For more details see [49]. The solutions of the DMFT equations for the interacting DOS depend crucially on the ratio J_l/W_l. The critical value for the formation of well-defined IBs[6], corresponding to carrier spins locally parallel to Mn spins, is $J_l/W_l \sim 0.33$. In our study, the domain $J_l/W_l < 0.33$ is referred usually to as 'weak coupling', while $0.33 < \sim J_l/W_l < \sim 0.5$ is the 'intermediate coupling'. The most interesting physics is observed at the boundary between these two regimes, i.e. when the IBs are not completely separated from the valence bands.

In figure 7, we show T_C versus p, for different ratios J_2/J_1 and at fixed $W_2/W_1 = 1$ and $J_1/W_1 = 0.5$, a situation corresponding to the existence of a well-defined $l = 1$ IB (although

---

[6] The term 'impurity band' is widely used in the DMS literature (see e.g. [61, 62]), although it should not be confused with the same term used in non-magnetic doped semiconductor literature. Perhaps 'exchange split valence band' could be a better terminology.
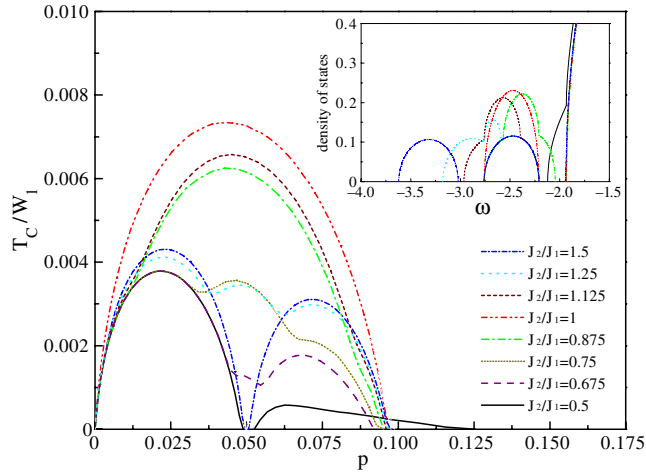
Figure 7. T_C versus the carrier concentration p, at various J_2/J_1. Here, $x = 0.05$, $W_1/W_2 = 1$, and $J_1/W_1 = 0.5$. The inset shows the corresponding low-temperature interacting DOS (from [49]).
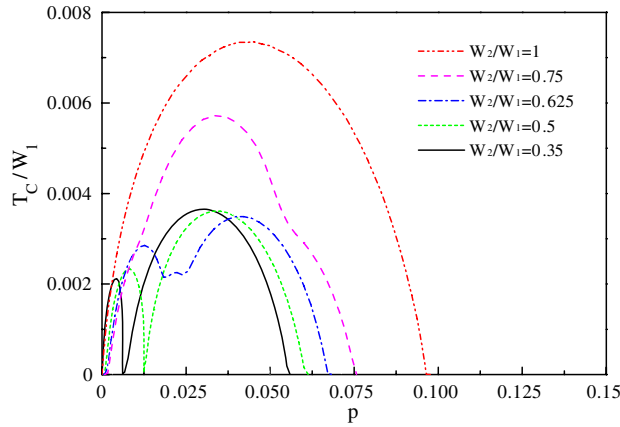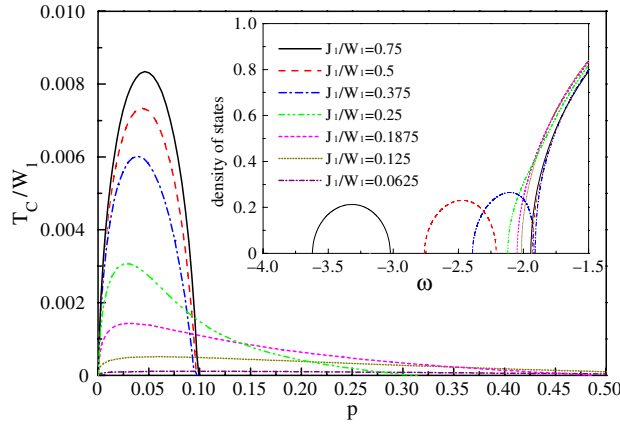

Figure 8. T_C versus p at different ratios W_2/W_1, fixing $J_1 = J_2 = 2$. Here $x = 0.05$ (from [49]).

$p \leqslant x$ in real DMSs, the case $p > x$ is also studied for completeness, as done in [54]). The inset shows the total interacting DOS evolution. The IBs overlap if $|J_2/W_2 - J_1/W_1| < 0.5$. If the IBs do not overlap, then each one determines T_C separately, causing the double-peak structure observed for some J_2/J_1 ratios. The band with the largest J_l/W_l is filled first, for smaller μ. At all p, we found that T_C is maximum when $J_2/J_1 = 1$, namely when the IBs fully overlap. Once the bands decouple, the value for T_C matches one-band model results.

Let us consider now how changes in bandwidths influence T_C. In figure 8, we show T_C versus p for different W_2/W_1, at fixed $J_1/W_1 = 0.5$ (intermediate coupling), and with $J_2/J_1 = 1$.[7] At small W_2/W_1 the second IB will be located in a region of ω smaller (i.e. farther from the valence bands) than the energy interval occupied by the $l = 1$ IB. Hence, the $l = 2$ IB will be the first to be filled. Decreasing J_2/W_2, the second band moves to the right on the ω axis, towards the location of the first band. While the bands are still separated, each gives its

---

[7] The relative position of the bands is fixed by shifting the $l = 2$ valence band numerically such that both valence bands start at the same energy, to mimic the degeneracy of the light and heavy bands of GaAs at the Γ point.

Figure 9. T_C versus p at different ratios J_1/W_1, obtained using DMFT. The parameters x, W_1, W_2, and J_1 are as in figure 7. The inset shows the low-temperature interacting DOS (from [49]).

own contribution to T_C. The curves with $W_2/W_1 = 0.35$ and 0.5 correspond to decoupled IBs, while those with $W_2/W_1 = 0.625$ and 0.75 correspond to partially overlapping bands. Again, T_C is maximized at all fillings when the bands fully overlap ($W_2/W_1 = 1$), in good agreement with [50]. Although $W_2/W_1 = 1$ is not realistic in DMSs, we come to the conclusion that Mn-doped materials with a relatively small heavy–light mass ratio will favour a higher T_C.

Now it is established that T_C is maximal for all p when $J_2/J_1 = 1$ and $W_2/W_1 = 1$, let us analyse T_C versus p when J_1/W_1 varies. The results for T_C, and total interacting DOS, are in figure 9. At small coupling $J_1/W_1 \ll 0.33$, T_C is small, flat, and much extended on the p axis, results qualitatively similar to those found for one band [54]. However, at intermediate coupling, T_C is non-zero in the range from $p = 0$ to $p = 2x$, adopting a parabolic form with the maximum at $p \cong x$, in contrast with the one-band model which gives a null T_C when $p \cong x$. The explanation is straightforward: at $p = x$ in the one-band model the IB is fully occupied, leading to a vanishing T_C, but for the same p in the two-band model both bands are half filled, which ultimately leads to the highest value for T_C.

Concluding, the critical temperature T_C is maximized at intermediate couplings and for all carrier densities p when $J_1/J_2 = 1$ and $W_1/W_2 = 1$. The maximum T_C is obtained at $p \cong x$, in contrast with the one-band model which shows a vanishing T_C at the same doping. In addition, T_C at filling $p \cong x/2$ in the one-band case is smaller than with two bands by a factor ~ 2. In view of the simplicity of the main results, it is clear that adding an extra band to the calculations will only lead to a further increase in T_C when all the IBs overlap.

The approach described here is also quantitative. In fact, using realistic mean values specific to GaAs such as $p = 0.005$, a bandwidth ~ 10 eV ($t_1 \approx 2.5$ eV), $t_2 = (1/9)t_1$, and assuming $J_1/t_1 = 1$ and $J_1 = J_2$, we obtain $T_C \approx 175$ K, i.e. within the experimental range. While this agreement with experiment [48] may be accidental, the trends are reliable and the result improves upon single-band estimations. Moreover, for optimal $t_2/t_1 = 1$ and $J_1/t_1 = 2$, the T_C raises to ~ 340 K, even at small $p = 0.005$, setting the upper bound for DMSs under a two-band model description using a cubic lattice.

Our model presents several simplifications. For example, the Coulomb attraction by acceptors is not included, thereby neglecting the dominant energy of impurity states. The on-site Coulomb repulsion term $U \sum_i n_{i\uparrow} n_{i\downarrow}$, and the nearest-neighbour one $V \sum_{\langle ij \rangle} n_i n_j$ (where $n_i = n_{i\uparrow} + n_{i\downarrow}$), are not accounted for in the Hamiltonian (2). While the value of T_C is clearly

affected by the Coulomb interactions, our model is still able to capture the main qualitative trends since the value of V, for instance, is comparable with the hopping and smaller than the coupling. On the other hand, the influence on T_C of the nearest-neighbour Coulomb repulsion may be suppressed by the exchange effect among bands that is expected to induce a boost of T_C once the off-diagonal hopping terms are accounted for.

5. Conclusions

The study presented in this brief review paper has covered several materials. In all of them, the effect of strong electronic correlations is important. For instance:

(i) Electron–electron and electron–phonon correlations play a crucial role in transport and other properties of nanostructures, as explained in section 2. Many of the observed effects usually occur only in these nanoscopic structures and not in the bulk. We have discussed new techniques, with particular emphasis on numerical methods, and have presented various results that can be obtained with these methods.

(ii) In section 3, a recent Monte Carlo study of the resistivity in a one-orbital spin-fermion (or double-exchange) model for manganites was briefly reviewed. A study of a two-orbital model for manganites has also been carried out (not discussed here but for details the reader can consult [38]). The overall conclusion is that its behavior is similar to that of the one-orbital model. Since these results are themselves also similar to experiments, our effort and those of other groups provide evidence that the theoretical studies that have focused on the regime of competition between a metal and an insulator are on the right track towards a full explanation of the CMR phenomenon. Both with one and two orbitals, quenched disorder is important in enlarging the magnitude of the effects and broadening its range in parameter space, thus avoiding the fine tuning of couplings needed in the clean limit.

The results reviewed in section 3 described mainly ferromagnetic phases both metallic and insulating. An area of study left for near future research is the important situation of non-ferromagnetic insulating phases competing with the ferromagnetic metallic regime. In fact, there has been some results concerning the effect of disorder on the insulating phases of manganites [60]. But more work is needed to address the effect of the superexchange coupling on the metal to insulator transition and on the formation of charge-ordered states.

(iii) Finally, the models and methods presented in section 4 can be used to search for diluted magnetic semiconductors with even higher T_C than currently known. Our results suggest that semiconductors with the heavy-to-light-hole mass ratio the closest to 1, such as AlAs, could have the highest T_C if the couplings J could be tuned to its optimal value. The present effort paves the way toward future non-perturbative studies of DMS models using realistic zinc blende lattices, and points towards procedures to a further increase of the Curie temperature.

Overall, it can be concluded that the study of strongly correlated electronic systems continues providing interesting results, surprises, and soon may develop into an area of investigations with potential for real applications. Research in this field should continue to be strongly pursued by the condensed matter community.

References

[1] Meir Y, Wingreen N S and Lee P A 1991 *Phys. Rev. Lett.* **66** 3048
[2] Meirav U, Kastner M A and Wind S J 1990 *Phys. Rev. Lett.* **65** 771
[3] Park J, Pasupathy A N, Goldsmith J I, Chang C, Yaish Y, Petta J R, Rinkoski M, Sentha J P, Abruna H D, McEuen P L and Ralph D C 2002 *Nature* **417** 722
[4] Liang W, Shores M P, Bockrath M, Long J R and Park H 2002 *Nature* **417** 725
[5] Glazman L I and Raikh M E 1988 *JETP Lett.* **47** 452
[6] Ng T K and Lee P A 1988 *Phys. Rev. Lett.* **61** 1768
[7] Meir Y, Wingreen N S and Lee P A 1993 *Phys. Rev. Lett.* **70** 2601
[8] Goldhaber-Gordon D, Shtrikman H, Mahalu D, Abusch-Magder U, Meirav U and Kastner M A 1998 *Nature* **391** 156
[9] Yu L H and Natelson D 2004 *Nano Lett.* **4** 79
[10] Cobden D H, Nygard J and Lindelof P E 2000 *Nature* **408** 342
[11] Chang A M, Jeong H and Melloch M R 2001 *Science* **293** 2221
[12] Georges A and Meir Y 1999 *Phys. Rev. Lett.* **82** 3508
[13] Büsser C A, Anda E V, Lima A L, Davidovich M A and Chiappe G 2000 *Phys. Rev.* B **62** 9907
[14] Martins G B, Büsser C A, Al-Hassanieh K A, Moreo A and Dagotto E 2005 *Phys. Rev. Lett.* **94** 026804
[15] Sasaki S, De Franceschi S, Elzerman J M, van der Weil W G, Eto M, Tarucha S and Kouwenhoven L P 2000 *Nature* **405** 764
[16] Jarillo-Herrero P, Kong J, van der Zant H S J, Dekker C, Kouwenhoven L P and De Franceschi S 2005 *Nature* **434** 488
[17] Al-Hassanieh K A, Büsser C A, Martins G B and Dagotto E 2005 *Phys. Rev. Lett.* **95** 256807
[18] Mitra A, Aleiner I and Millis A J 2004 *Phys. Rev.* B **69** 245302
[19] Cornaglia P S, Ness H and Grempel D R 2004 *Phys. Rev. Lett.* **93** 147201
[20] Park H, Park J, Lim A K L, Anderson E H, Alivisatos A P and McEuen P L 2000 *Nature* **407** 57
[21] Yu L H, Keane Z K, Ciszek J W, Cheng L, Stewart M P, Tour J M and Natelson D 2004 *Phys. Rev. Lett.* **93** 266802
[22] Al-Hassanieh K A, Feiguin A E, Riera J A, Büsser C A and Dagotto E 2006 *Phys. Rev.* B **73** 195304
[23] Schneider G and Schmitteckert P 2006 *Preprint* cond-mat/0601389
[24] Martins G B, Büsser C A, Al-Hassanieh K A, Anda E V, Moreo A and Dagotto E 2006 *Phys. Rev. Lett.* **96** 066802
[25] Craig N J, Taylor J M, Lester E A, Marcus C M, Hanson M P and Gossard A C 2004 *Science* **304** 565
[26] Büsser C A, Martins G B, Al-Hassanieh K A, Moreo A and Dagotto E 2004 *Phys. Rev.* B **70** 245303
[27] Millis A, Littlewood P and Shraiman B 1995 *Phys. Rev. Lett.* **74** 5144
[28] Calderón M J, Vergés J A and Brey L 1999 Conductance as a function of temperature in the double-exchange model *Phys. Rev.* B **59** 4170
[29] Moreo A, Yunoki S and Dagotto E 1999 Phase separation scenario for manganese oxides and related materials *Science* **283** 2034
[30] Dagotto E 2002 *Nanoscale Phase Separation and Colossal Magnetoresistance* (Berlin: Springer)
[31] Dagotto E 2005 *Science* **309** 258
[32] Yunoki S, Hu J, Malvezzi A, Moreo A, Furukawa N and Dagotto E 1998 *Phys. Rev. Lett.* **80** 845
[33] Dagotto E, Hotta T and Moreo A 2001 Colossal magnetoresistant materials: the key role of phase separation *Phys. Rep.* **344** 1
[34] Mayr M, Alvarez G and Dagotto E 2002 Global versus local ferromagnetism in a model for diluted magnetic semiconductors studied with Monte Carlo techniques *Phys. Rev.* B **65** 241202
[35] Burgy J, Mayr M, Martin-Mayor V, Moreo A and Dagotto E 2001 Colossal effects in transition metal oxides caused by intrinsic inhomogeneities *Phys. Rev. Lett.* **87** 277202
[36] Burgy J, Moreo A and Dagotto E 2004 *Phys. Rev. Lett.* **92** 097202
[37] Verges J A, Martin-Mayor V and Brey L 2002 *Phys. Rev. Lett.* **88** 136401
[38] Şen C, Alvarez G, Aliaga H and Dagotto E 2006 *Phys. Rev.* B **73** 224441
[39] Kumar S and Majumdar P 2005 *Phys. Rev. Lett.* **94** 136601
[40] Kumar S and Majumdar P 2006 Insulator-metal phase diagram of the optimally doped manganites from the disordered holstein-double exchange model *Phys. Rev. Lett.* **96** 016602
[41] Vergés J A 1999 Computational implementation of the Kubo formula for the static conductance: application to two-dimensional quantum dots *Comput. Phys. Commun.* **118** 71

[42] Metzner W and Vollhardt D 1989 *Phys. Rev. Lett.* **324** 62
[43] Müller-Hartmann E 1989 *Z. Phys.* B **74** 507
[44] Georges A, Kotliar G, Krauth W and Rozenberg M J 1996 *Rev. Mod. Phys.* **68** 13
[45] Wolff S A 2001 *Science* **294** 1488
[46] Zutic I, Fabian J and Das Sarma S 2004 Spintronics: fundamentals and applications *Rev. Mod. Phys.* **76** 323
[47] Ohno H, Shen A, Matsukura F, Oiwa A, Endo A, Katsumoto S and Iye Y 1996 (Ga,Mn)As: a new diluted magnetic semiconductor based on GaAs *Appl. Phys. Lett.* **69** 363
[48] Ohno H 1998 Making nonmagnetic semiconductors ferromagnetic *Science* **281** 951
[49] Popescu F, Yildirim Y, Alvarez G, Moreo A and Dagotto E 2006 *Phys. Rev.* B **73** 075206
[50] Aryanpour K, Moreno J, Jarrell M and Fishman R S 2005 *Phys. Rev.* B **72** 045343
[51] Zaránd G and Jankó B 2002 *Phys. Rev. Lett.* **89** 047201
[52] Moreno J, Fishman R S and Jarrell M 2006 *Phys. Rev. Lett.* **96** 237204
[53] Nazmul A M, Amemiya T, Shuto Y, Sugahara S and Tanaka M 2005 *Phys. Rev. Lett.* **95** 017201
[54] Chattopadhyay A, Das Sarma S and Millis A J 2001 Transition temperature of ferromagnetic semiconductors: a dynamical mean field study *Phys. Rev. Lett.* **87** 2272022
[55] Alvarez G, Mayr M and Dagotto E 2002 Phase diagram of a model for diluted magnetic semiconductors beyond mean-field approximations *Phys. Rev. Lett.* **89** 277202
[56] Alvarez G and Dagotto E 2003 Single-band model for diluted magnetic semiconductors: dynamical and transport properties and relevance of clustered states *Phys. Rev.* B **68** 045202
[57] Sinova J, Jungwirth T, Eric Yang S-R, Kucera J and MacDonald A H 2002 Infrared conductivity of metallic (III,Mn)V ferromagnets *Phys. Rev.* B **66** 041202
[58] Jungwirth T, König J, Sinova J, Kucera J and MacDonald A H 2002 Curie temperature trends in (III,Mn)V ferromagnetic semiconductors *Phys. Rev.* B **66** 012402
[59] Popescu F, Şen C and Dagotto E 2006 *Phys. Rev.* B **73** 180404(R)
[60] Alvarez G, Aliaga H, Şen C and Dagotto E 2006 *Phys. Rev.* B **73** 224426
[61] Berciu M and Bhatt R N 2001 *Phys. Rev. Lett.* **87** 107203
[62] Okabayashi J, Kimura A, Rader O, Mizokawa T, Fujimori A, Hayashi T and Tanaka M 2001 *Phys. Rev.* B **64** 125304